SAND2018-13540C

Modeling Empirical Size Relationships on Load-Displacement Behavior and Failure in Threaded Fasteners

Peter W. Grimmer[1], John P. Mersch[1], Jeffrey A. Smith[1]
Sandia National Laboratories, Albuquerque, NM, 87185

Yuriy B. Veytskin[2]
Savannah River National Laboratory, Aiken, SC, 29808

Donald F. Susan[3]
Sandia National Laboratories, Albuquerque, NM, 87185

A collaborative testing and analysis effort investigating the effects of threaded fastener size on load-displacement behavior and failure was conducted to inform the modeling of threaded connections. A series of quasistatic tension tests were performed on #00, #02, #04, #06 and #4 (1/4") A286 stainless steel fasteners (NAS1351N00-4, NAS1352N02-6, NAS1352N04-8, NAS1352N06-10, and NAS1352N4-24, respectively) to provide calibration and validation data for the analysis portion of the study. The data obtained from the testing series reveals that the size of the fastener may influence the characteristic stress-strain response, as the failure strains and ultimate loads varied between the smaller (#00 and #02) and larger (#04, #06, and #4) fasteners. These results motivated the construction of high-fidelity finite element models to investigate the underlying mechanics of these responses. Two threaded fastener models, one with axisymmetric threads and the other with full 3D helical threads, were calibrated to subsets of the data to compare modeling approaches, analyze fastener material properties, and assess how well these calibrated properties extend to fasteners of varying sizes and if trends exist that can inform future best modeling practices. The modeling results are complemented with a microstructural analysis to further investigate the root cause of size effects observed in the experimentally obtained load-displacement curves. These analyses are intended to inform and guide reduced-order modeling approaches that can be incorporated in system level analyses of abnormal environments where modeling fidelity is limited and each component is not always testable, but models must still capture fastener behavior up to and including failure. This complimentary testing and analysis study identifies differences in the characteristic stress-strain response of varying sized fasteners, provides microstructural evidence to support these variations, evaluates our ability to extrapolate calibrated properties to different sized fasteners, and ultimately further educates the analysis community on the robustness of fastener modeling.

Nomenclature

DVRT	=	Differential Variable Reluctance Transducer
LVDT	=	Linear Variable Differential Transformer
ϵ_p	=	equivalent plastic strain
h	=	hardening parameter
r	=	recovery parameter
y	=	initial yield stress

[1] R&D S&E Mechanical Engineering, Component Science & Mechanics, PO Box 5800, MS0346
[2] Senior Scientist, Advanced Characterization & Processing Group, Savannah River National Laboratory
[3] R&D S&E Materials Science, Metallurgy & Materials Joining, PO Box 5800, MS0886

I. Introduction

Computational capacity continues to grow, and the engineering analysis community is increasingly relying on the simulation of large, full-system structures to make important decisions – often in the absence of direct test data. The integrity of these simulations has thus become a key component of the engineering design and qualification process. However, these structures can be so complicated that testing each individual component to obtain material parameters for constitutive models is infeasible. Threaded fasteners are a common example of these types of components as they are a prevalent joint connector and may vary significantly in size and application throughout the structure. Therefore, it is desirable to understand the behavior of threaded fasteners to changes in size to reliably represent these important connections in our full-system analysis models. This problem is further complicated by the requirements typically imposed on modeling fidelity in system level models, as the fastener mesh must be conducive to maintaining the feasibility of the larger finite element simulation. We are thus seeking to be more predictive of fastener size effects while ultimately utilizing reduced-order models for these threaded connections.

This effort is part of a larger collaborative study to explore best practices for the testing and modeling of threaded fasteners. Previous work has investigated extrapolating constitutive models calibrated to quasistatic test data to dynamic environments[1], identifying sensitivities in the testing-calibration-modeling process[2], and the applicability of pure material properties when used for fasteners of the same material[3]. These studies provided valuable insights toward improving threaded fastener modeling, but many areas have yet to be researched that can further improve our predictive modeling capabilities.

Similar fastener data to what is presented in this paper was leveraged for our most recent study[3] and general size effect trends were identified, but the reduced-order fastener models could not independently predict the changes in yield strength and failure strain as fastener size increased. This paper focuses on further understanding load-displacement behavior of varying sized fasteners through a collaborative testing and high-fidelity analysis effort. A series of quasistatic tension tests were performed on #00, #02, #04 #06 and #4 (1/4") A286 stainless steel fasteners (NAS1351N00-4, NAS1352N02-6, NAS1352N04-8, NAS1352N06-10, and NAS1352N4-24, respectively) and high-fidelity threaded fastener models were developed to further explore the underlying mechanics governing the problem. This analysis is supported by microstructural characterization of the fasteners to help determine the cause of the size effects observed in the testing series. The high-fidelity analysis models are meant to guide reduced-order fastener modeling in system level finite element analyses, especially abnormal environment simulations where predicting failure is important. Not all components can be tested in complex, system level structures, and analysts must rely on extrapolated properties to complete their model. Without any guidance on how fastener properties can vary with loading type, loading rate, and size, the system level model may contain unacceptable amounts of uncertainty and the robustness of the analysis may be limited.

II. Test Setup

Fixtures were designed and built to test A286 fasteners of size #00, #02, #04, #06, and #4 in quasistatic tension. These fasteners are shown in Fig. 1. For additional fastener details and dimensions, refer to the NAS1351 and NAS1352 datasheets[4],[5]. Full documentation of the test setup and procedure is provided in a complementary paper[6], but a brief description is included here as well.

Fig. 1 A286 Fasteners: (From Left) Size #00, #02, #04, #06, and #4.

Fig. 2 Test Setup Photos.

Photographs of the test setup are shown in Fig. 2 and a drawing of the quasistatic tension test apparatus is shown in Fig. 3. The test fixturing includes the 4340 steel bushing holders, 4340 steel bushings (interchangeable for each size fastener), and A286 stainless steel fastener. Displacement data for each test is collected at multiple locations by four differential variable reluctance transducers ("DVRTs") and four Linear Variable Differential Transformers ("LVDTs"). The DVRTs are located in the top bushing 0.75 in (19.1 mm) from the axis of the fixture and measure the displaced gap between the top and bottom bushings. The LVDTs are located outside of the test fixtures (see Fig. 2, Fig. 3 and Fig. 4) and measure the displacement between the mounted steel blocks attached to the top and bottom bushing holders. All tests were performed on non-preloaded fasteners which were "hand-tightened" with small, regulated torque wrench values unique to each fastener size.

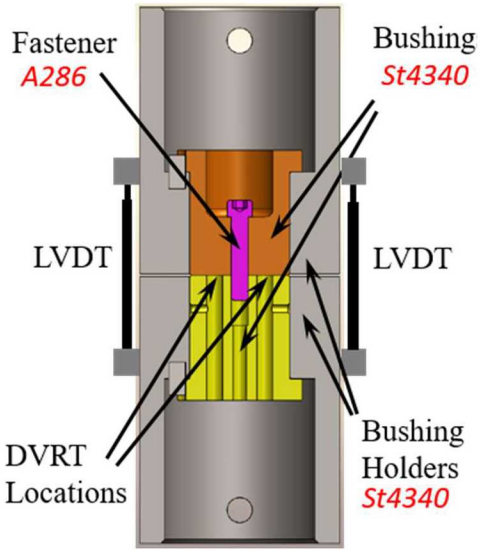

Fig. 3 Quasistatic Tension Test Setup.

III. Test Results

Quasistatic tension tests were performed using the testing apparatus described in section II on five different sized fasteners: #00, #02, #04, #06, and #4. Load-displacement results are shown in Fig. 5. Note that in the legend, the shorthand "S##" stands for "Size ##". A complete summary of the test setup, procedure, and results will be provided in a paper/presentation at SEM[6].

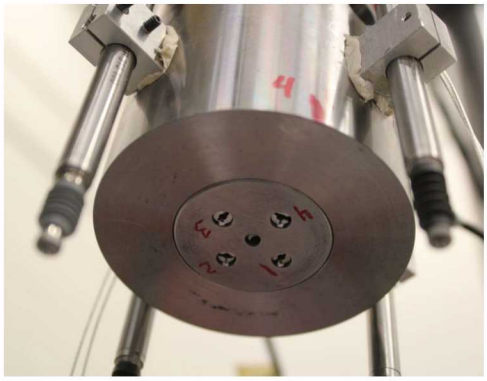

Fig. 4 DVRTs in the Top Bushing.

The load-displacement responses of the different sized fasteners are qualitatively similar and the peak loads increase with size in a predictable way, but the failure displacements do not seem to follow any discernable trend. However, trends for these tests can be difficult to evaluate in load-displacement space because the area and gage length of the fasteners are varying. Therefore, the load-displacement responses are converted to stress-strain using the threaded tensile stress area provided in ASME B1.1-2003[7] and the gage length of the tested fastener. Note that the #4 fastener has a large non-threaded region (Fig. 1). After consideration, this length was removed from the gage length because we believe it is only accommodating elastic strains and not significantly contributing to the displacement of the specimen. The stress-strain curves of each fastener are shown in Fig. 6. When analyzing the data in stress-strain space, it is easier to observe the large difference between the behavior of the #00

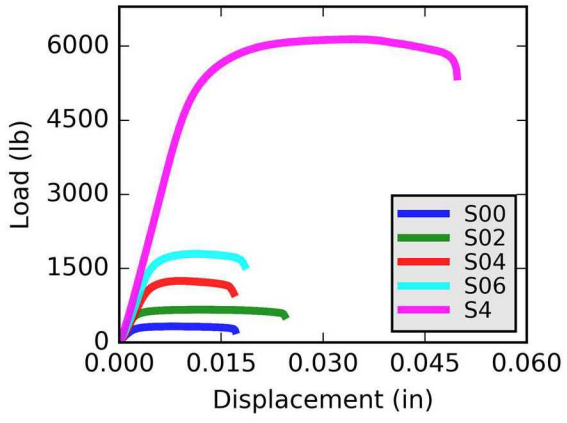

Fig. 5 Quasistatic Tension Test Results – Load-Displacement.

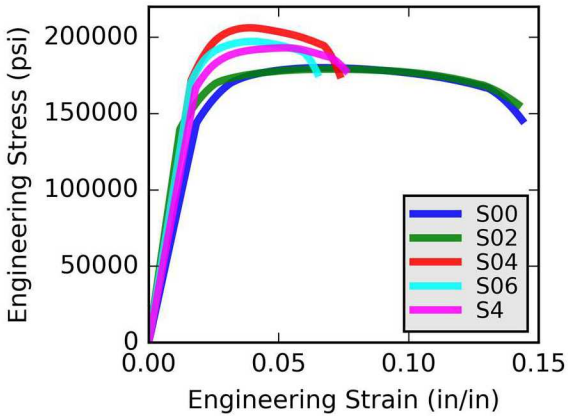

Fig. 6 Quasistatic Tension Test Results – Engineering Stress-Strain.

and #02 compared to the #04, #06, and #4 fasteners – the smallest two fasteners have a lower yield stress and more ductility than the larger fasteners. Energy absorption is an important quantity in failure prediction, so a measure of the energy density dissipated by each fastener is computed by calculating the area under the curves (using Simpson's Rule[8]) in Fig. 6. The #00 and #02 fasteners that exhibit lower yield and higher ductility have failure energies of 23.1 lbf-in/in^3 and 23.4 lbf-in/in^3, respectively, while the #04, #06, and #4 fasteners that have higher yield stress and lower ductility have failure energies of 12.9 lbf-in/in^3, 10.8 lbf-in/in^3, and 12.5 lbf-in/in^3, respectively, approximately a 50% reduction in energy absorption.

The stark differences between the strength and ductility of the #00 and #02 fasteners and the #04, #06, and #4 fasteners motivated a microstructural investigation. Electron backscatter diffraction (EBSD) maps, captured from a scanning electron microscope, of an untested #02 and #06 fastener are shown in Fig. 7 and Fig. 8, respectively. Note Fig. 7 and Fig. 8 show the Inverse Pole Figures with respect to the "x direction" (IPF X), which is along the axis of the fastener. The #02 fastener map is morphologically (structurally) representative of the #00 and #02 group, and the #06 fastener map is morphologically representative of the #04 and #06. No EBSD has been performed on the ¼" specimens. The grain structure is very different in the two fasteners, as the grains in the #06 tend to be elongated with a columnar pattern, and have evidence of cold work through the preferential axis orientation in the #06 fastener whereas the grains in the #02 fastener are equiaxed, indicating an annealed structure (as opposed to cold-worked), with more clearly defined grain boundaries in the EBSD map. Note that, while the grain structure indicates a cold-worked vs. annealed structure, all of the fasteners have been subsequently precipitation strengthened (age hardened) to a high-strength condition. In both Fig. 7 and Fig. 8, the distributions of the colors of the inverse pole figures are

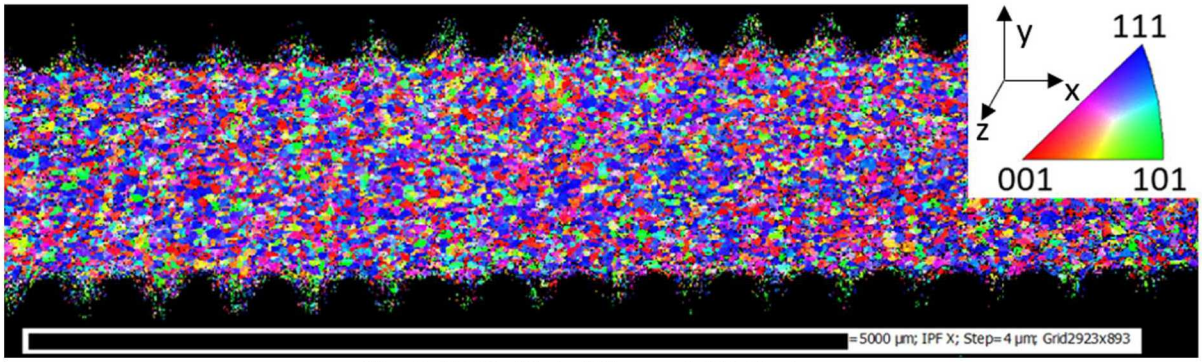

Fig. 7 EBSD Plot of Untested #02 Fastener.

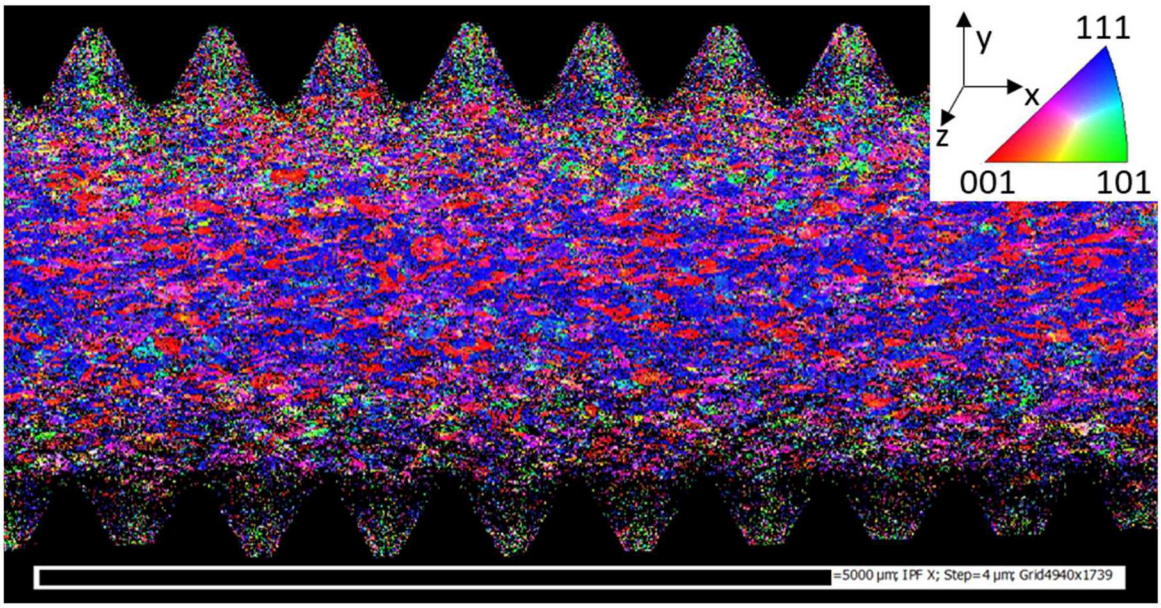

Fig. 8 EBSD Plot of Untested #06 Fastener.

similar, suggesting that the crystallographic grain orientations are preferred to similar extents in both fasteners, however Fig. 8 shows more affinity for the <1 1 1> Euler-based axis (blue) and <001> (red) along the axis of the cold-worked fastener while <1 0 1> (green) is less prevalent, especially in the central region of the fastener. It is known that cold working deforms metal grain structures, as observed in Fig. 8, and creates a "locking effect" from the entanglement of generated dislocations, which causes increased yield and ultimate tensile strengths and reduced deformation, all of which are represented in Fig. 6 when comparing the #00 and #02 "annealed" fastener group to the #04 and #06 "cold worked" fastener group. It is known that annealing increases ductility by reducing the number of dislocations and increasing the number of slip conditions at grain boundaries, and this increased ductility is represented by an increased strain to failure for the #00 and #02 fastener group in Fig. 6. The correlation between the microstructure and load-displacement behavior suggests that EBSD mapping of the #4 fastener will reveal it is structurally similar to the #04 and #06.

IV. Analysis Models

Finite element analysis models were constructed for the #02 and the #06 test setups and are described in the following sections. Analyses are performed with two different high-fidelity models of a threaded fastener inside the bushings – an axisymmetric model and a full 3D model with helical threads. Both fastener models use an elastic-plastic material model.

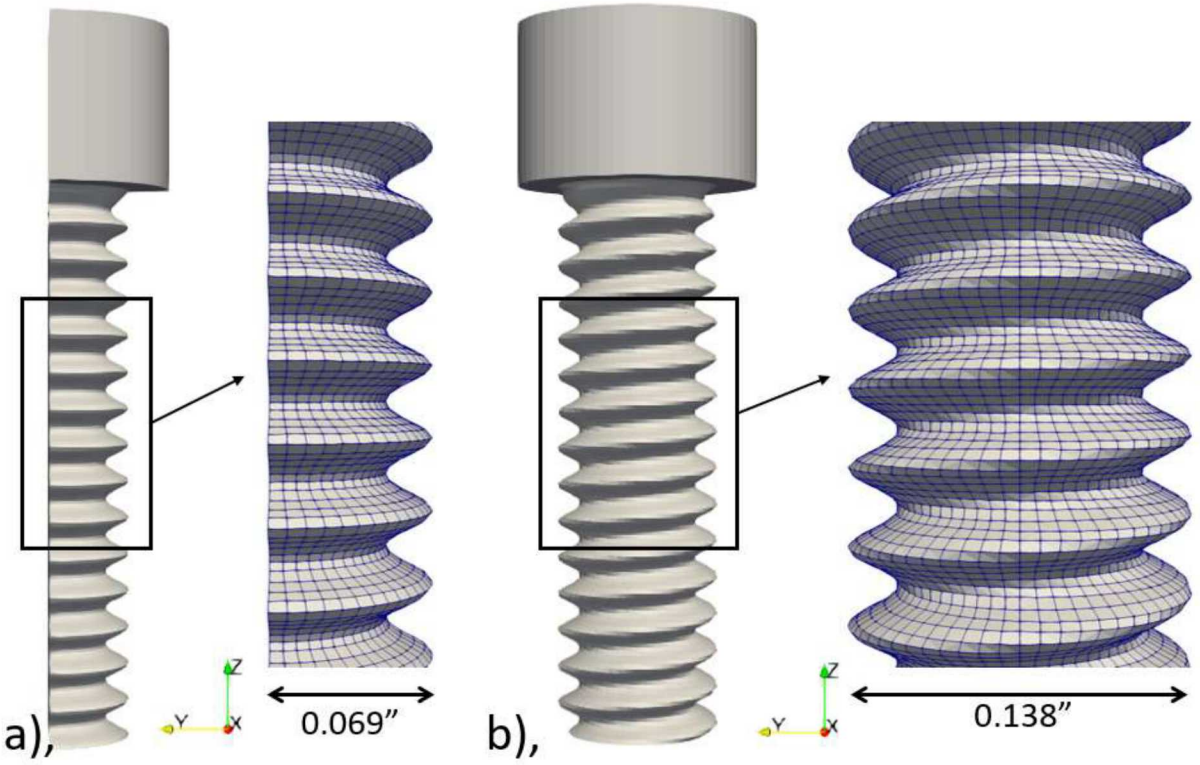

Fig. 9 Finite Element Models of #06 Fastener. A.) Axisymmetric Thread Wedge Model, B.) Helical Thread Fully 3D Model.

A. Threaded Fastener Models

An axisymmetric threaded model is constructed of one-quarter of the fastener (Fig. 9a) utilizing symmetry of the design. Here, the term "axisymmetric" refers to the thread form modeled, as they are not helical but rather discrete threads. The shape of the threads is derived from the UNRC thread form, capturing the correct inner and outer diameters, and the number of threads per inch for each fastener, but neglects the helical pattern of the threads.

A fully 3D helical model is also constructed based on the UNRC fastener geometry and is shown in Fig. 9b. The geometry of the shank is created by revolving a circular cross section in a helical path along the axis of the fastener.

The mesh is then generated by partitioning the geometry into thin quartered axial sections and sweeping the mesh along the axis of the fastener. This method of meshing a helical fastener is very similar to another method found in the literature[9], but slightly deviates from the non-circular cross-section incorporated in their paper that better represents the true cross-section and thread form. Other methods of revolving threads and meshing them separately from the inside of the shank lead to difficulties in contiguously meshing the center, as well as problems with resolving the head geometry, while this method allows for the entire fastener to be contiguously swept with hexahedral elements and allows for a smooth runout thread where the threads meet the head.

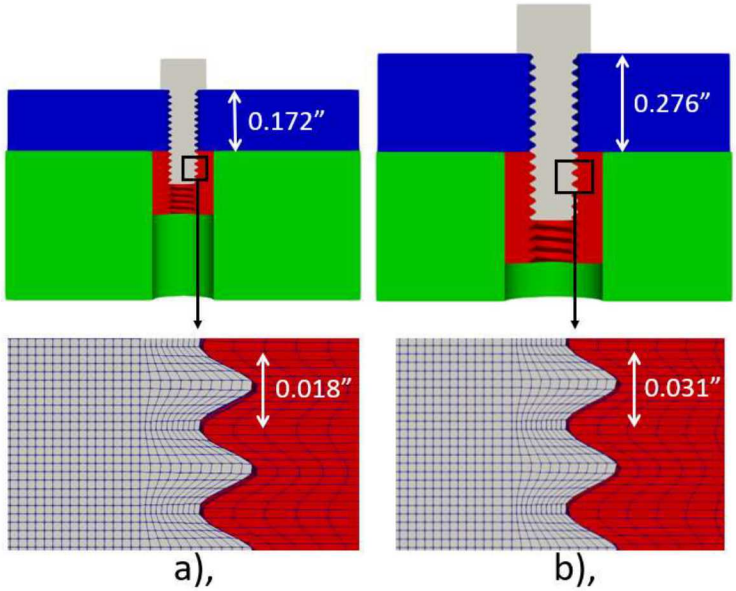

Fig. 10 Finite Element Models of Test Setups (Cross Section). A.) #02 Helical Thread, B.) #06 Helical Thread.

Portions of the bushings from the tests (Fig. 3) are included in the analysis model to reproduce realistic boundary conditions and approximate the experimentally measured DVRT displacements. The helical threaded analysis models of the #02 and #06 fasteners are shown in Figs. 10a and 10b, respectively. The axisymmetric models are similar, but are quarter-symmetric models with symmetry boundary conditions (see Fig. 9a). The mating portion of the bottom threaded bushing (shown in red in Fig. 10) has similar element size to the fastener, with its mating surface to the threads of the fastener slightly offset to model the clearance between internal and external threads. The red mating section is embedded into a more coarsely meshed bottom bushing (shown in green in Fig 10) section with tied contact. Coulomb frictional contact is modeled between the fastener and the bottom bushing, with a friction coefficient of 0.15. Displacement boundary conditions are applied to the outer surfaces of the top (prescribed displacement ramp) and bottom (fixed displacement) bushing sections, and load is allowed to develop through the fastener. The prescribed displacement on the top bushing approximates the locally measured DVRT displacements in the test. Simulations are performed using the implicit module of the code Sierra/SM[10] and 8-node, uniform gradient hexahedral elements are used for all geometry.

B. Fastener Material Model

An elastic-plastic, rate-independent, isotropic-hardening, J2 plasticity model is used for the fastener geometry. The hardening curve is defined by a 3-parameter hardening-minus-recovery function:

$$\sigma_y = y + \frac{h}{r}[1 - \exp(-r\epsilon_p)] \tag{1}$$

Where σ_y is the current yield stress, y is the initial yield stress, h is the hardening parameter that defines the initial hardening modulus, r is the recovery parameter that governs the rate at which the hardening modulus asymptotes to zero, and ϵ_p is the equivalent plastic strain. The three parameters y, h, and r can be selected such that the fastener model's load-displacement behavior matches the corresponding test data up until the sharp reduction in load indicating ultimate failure. Attempting to capture the load-displacement behavior during fracture is beyond the scope of this work. Instead, a simple death criterion is implemented based on a critical value of equivalent plastic strain that causes the model to fail at a displacement consistent with test results.

V. Analysis Results

A. Calibrated Models

The #02 and #06 helical models were separately calibrated to their corresponding load-displacement test results using the prescribed displacement on the top bushing from the analysis model and the DVRT output from the test. The calibrated responses and the analogous test results are shown in Fig. 11. In order to capture ultimate failure, the model is initially run without any element death. Then, the max equivalent plastic strain in the model (which occurs somewhere along the thread root) at the displacement where the load begins to drop in the test is used as the critical equivalent plastic strain for element death. The material parameters for both models are provided in Table 1. As expected, the #02 model has a lower yield stress and a higher critical equivalent plastic strain than the #06 model.

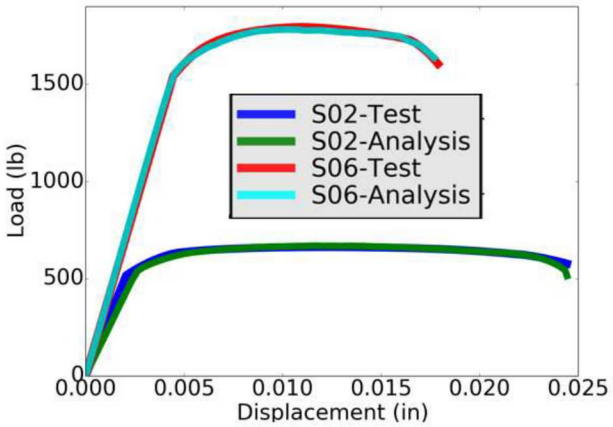

Fig. 11 Load-Displacement of Calibrated #02 and #06 Helical Models

Table 1 Calibrated Fastener Material Parameters

Model	y	h	r	$\epsilon_{p,crit}$
#02	160,000 psi	1e+06	30	0.43
#06	185,000 psi	1e+06	120	0.17

B. Axisymmetric vs. Helical Thread Model

A comparison of the load-displacement responses between the axisymmetric and helical models, both run with the calibrated #06 material model parameters, is shown in Fig. 12. The models give essentially identical load-displacement outputs until elements at the thread roots begin to reach the critical equivalent plastic strain value and are killed (instantaneously assigned zero stiffness). The axisymmetric model has a varying cross-sectional area along the axis of the fastener, and fracture occurs at a minimum cross section area, perpendicular to the axis of the fastener. In contrast, every cross section of the helical model nominally has the same area, and the 3D helical geometry leads to a 3D fracture path. This allows the helical model to be "tougher" throughout the fracture process given the same constitutive model and failure criterion. This can be observed in Fig 13 as the axisymmetric model has more crack growth for a given displacement than the helical model (see circled areas of the fastener). While the axisymmetric model can be used to effectively capture behavior up to failure, the results deviate during the fracture process.

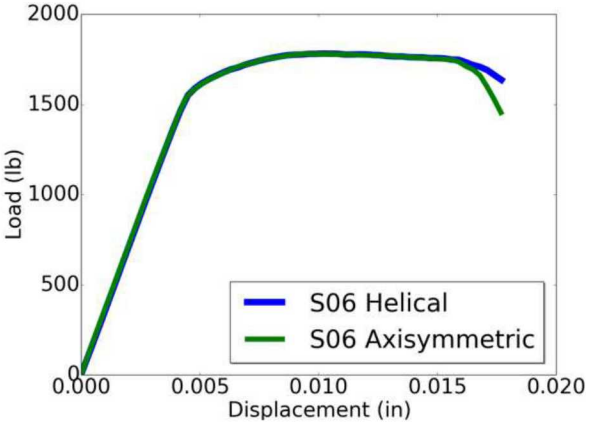

Fig. 12 #06 Axisymmetric vs Helical Models – Load-Displacement Responses

C. Extrapolation of Calibrated Model

Since it is infeasible to test all fasteners in a complex component or structure, our ability to predict the response of untested fasteners is vital to the performance of our system-level models. Thus, we used

the #06 material properties provided in Table 1 and applied them to the #02 analysis model to evaluate our ability to extrapolate fastener material properties to different sized fasteners. These results are shown in Fig. 14. The predicted response of the #02 (green in Fig 14.) has a slightly higher peak load than the test data and a much smaller displacement-to-failure, which is qualitatively similar to the #06 (teal in Fig 14.) response from which the material properties are obtained. Since the analysis prediction is essentially a scaled result of the #06 results, this suggests that the differences in the #02 and #06 load-displacement responses may be largely governed by the intrinsic material properties derived from the microstructure.

Depending on the quantity of interest, the extrapolated material properties may provide inadequate predictions. Although the peak loads are similar (706 lb and 663 lb for the #02 analysis and test results in Fig 14, respectively), the failure displacements differ by approximately a factor of two (0.013 in and 0.024 in for the #02 analysis and test results in Fig 14, respectively). In some cases this prediction can be non-conservative, as extrapolating #02 material properties will lead to more ductile predictions than observed in the #06 test data.

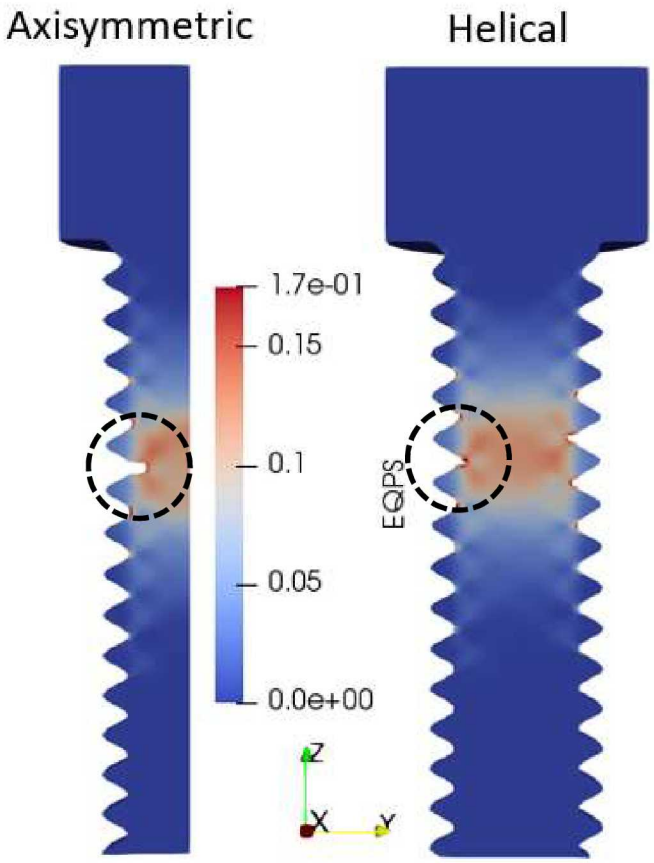

Fig. 13 Equivalent Plastic Strain Contours at Final Displacement for Each Model.

VI. Conclusions

Although these fasteners meet the same specification, there are stark differences in their load-displacement behavior – most notably between the small fasteners (#00 and #02) and larger fasteners (#04, #06, and #4). Generally, the smaller fasteners have a lower yield and ultimate stress with higher ductility whereas the larger fasteners display a higher yield and ultimate stress with lower ductility. These variations motivated a microstructural investigation, and the EBSD revealed fundamental differences in the microstructure and metallurgy that may contribute to the different behavior between the small and large fasteners. The grain structure is very different in the two fasteners, as the grains tend to be elongated and have evidence of cold work in the #06 fastener whereas the grains in the #02 are equiaxed indicating an annealed condition.

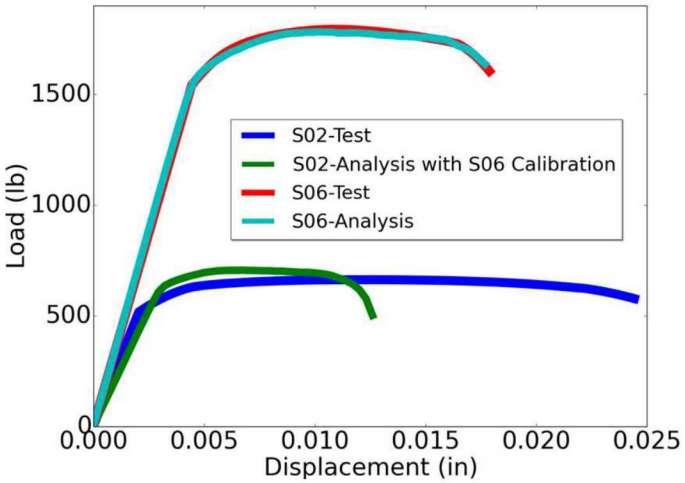

Fig. 14 #02 and #06 Load-Displacement Using the #02 Calibration

This observation complements the ductilities observed in the load-displacement results and is consistent with previous observations [3] that work hardening due to manufacturing and processing may affect some fasteners more than others and lead to this apparent discrepancy in material properties. One hypothesis is that the thread forming process may

affect different sized fastener differently – smaller fasteners may undergo more annealing, depending on the temperature of the thread rolling process. Another possibility is that the different sized fasteners are made from different sets of material that must be cold worked by varying amounts to achieve the specific fastener size. The material is obtained in the solution treated condition (ready for precipitation aging) and, depending on the initial size of the wire, the material must be cold worked to achieve specific sizes and properties[11]. After cold working to obtain the correct diameter and the general shape of a "blank", the precipitation aging heat treatment is applied. The precipitate distribution and number density are affected by the amount of cold work, i.e. prior dislocation density, in the material. Finally, the threads are rolled which may impart yet additional deformation and increased strength. The effects of these processing steps could manifest in different microstructures in different sized fasteners as shown in Fig. 7 and 8.

High fidelity finite element models of the fasteners were constructed to investigate the mechanics underlying the load-displacement performance of the fasteners. The models were calibrated such that their load-displacement response matched the measured load-displacement of the tested fasteners. The #02 model had a lower calibrated yield stress, and a higher calibrated critical equivalent plastic strain for element death than the #06 (Table 1), consistent with trends seen in the experimental engineering stress-strain curves. After the helical finite element models were calibrated, the #06 fastener was also modeled with an axisymmetric wedge geometry using the previously calibrated material model. The helical and axisymmetric geometries yielded the same load-displacement response until elements began to fail. After element failure begins, the fracture response of the two models qualitatively differs, with the axisymmetric model developing a straight crack across its thread root whereas the helical model has a three-dimensional crack path. While a simple element death criterion was used in this work, future efforts to predict fastener fracture using more accurate material damage models could use a helical thread form to elicit a more accurate fracture path. Finally, to demonstrate the error that may arise from a typical extrapolation from one size fastener to another similar untested fastener, the material model parameters calibrated to the #06 test data were input to the #02 helical finite element model. The results suggest that these types of extrapolations may not always provide accurate predictions, as the analysis model failure displacement was approximately half of the test data. Furthermore, the predicted load-displacement curve is qualitatively similar to the curve from which it was derived, indicating that even the high-fidelity model cannot elicit the differences observed in the test data.

A microstructural investigation revealed differences in the material of the #02 and #06 fasteners, which could explain the difference between the engineering stress-strain response of the smaller (#00 and #02) and larger (#04, #06, and #4) fasteners. The analysis results suggest that independent calibrations do not extrapolate well to fasteners that have different microstructures. Further, the analysis models did not reveal an underlying structural size effect that could guide extrapolation across sizes; rather, it appears that the differences in the load-displacement of the different sized fasteners are mostly dominated by differences in their inherent material properties. This consequently makes it difficult to guide fastener modeling in the absence of load-displacement test data or microstructural analysis that reveal fundamental characteristics of the material and its response. Future work should attempt to link specification and manufacturing information to the load-displacement response of a given fastener to improve blind predictions of fastener performance in the absence of direct test data on the fastener of interest.

Acknowledgments

The authors would like to thank John Emery of Sandia National Laboratories and Gustavo Castelluccio from Cranfield University for useful discussion, and Tom Bosiljevac of Sandia National Laboratories for performing the testing series and promoting a collaborative atmosphere. Sandia National Laboratories is a multimission laboratory managed and operated by National Technology and Engineering Solutions of Sandia, LLC, a wholly owned subsidiary of Honeywell International, Inc., for the U.S. Department of Energy's National Nuclear Security Administration under contract DE-NA0003525.

References

[1] Mersch, J. P., Smith, J. A., Johnson, E. P., "A CASE STUDY FOR THE LOW FIDELITY MODELING OF THREADED FASTENERS SUBJECT TO TENSILE LOADINGS AT LOW AND HIGH STRAIN RATES," *ASME Pressure Vessels and Piping Conference*, PVP2017-65518, ASME, Waikoloa, HI, 2017.

[2] Mersch, J. P., Smith, J. A., Johnson, E. P., Bosiljevac, T., "Evaluating the Performance of Fasteners Subjected to Multiple Loadings and Loading Rates and Identifying Sensitivities of the Modeling Process," *2018 AIAA/ASCE/AHS/ASC Structures, Structural Dynamics, and Materials Conference*, AIAA SciTech Forum, AIAA2018-1896, Kissimmee, FL, 2018.

[3]Grimmer, P., Barrios, A., Stossel, M., Mersch, J., Smith, J., Emery, J., Castelluccio, G., "Evaluation of the Nonlinear Mechanical Response of Threaded Fasteners," *2018 NAFEMS CAASE*, Cleveland, OH, 2018.

[4]AIA/NAS – Aerospace Industries Association of America Inc., 2016, “English -- SCREW, CAP, SOCKET HEAD, UNDRILLED AND DRILLED, PLAIN AND SELF-LOCKING, ALLOY STEEL, CORROSION-RESISTANT STEEL AND HEAT-RESISTANT STEEL, UNRF-3A - Rev 10”, AIA/NAS NAS1351.

[5]AIA/NAS – Aerospace Industries Association of America Inc., 2016, “English -- SCREW, CAP, SOCKET HEAD, UNDRILLED AND DRILLED, PLAIN AND SELF-LOCKING, ALLOY STEEL, CORROSION-RESISTANT STEEL AND HEAT-RESISTANT STEEL, UNRC-3A AND UNRC-2A - Rev 13”, AIA/NAS NAS1352.

[6]Veytskin, Y. B., Bosiljevac, T.R., “Testing the Influence of Size Effects on Load-Displacement Behavior and Failure in Threaded Fasteners” *2019 SEM Annual Conference*, Society for Experimental Mechanics, Reno, NV, 2019. *Submitted for Publication*

[7]ASME –The American Society of Mechanical Engineers, 2003, “Unified Inch Screw Threads (UN and UNR Thread Form)”, ASME B1.1-2003.

[8]“Integration and ODEs, *Scipy.org, 05/05/2018,* https://docs.scipy.org/doc/scipy/reference/integrate.html*, Accessed 10/2018,*

[9]T. Fukuoka and M. Nomura, “Proposition of Helical Thread Modeling With Accurate Geometry and Finite Element Analysis,” *J. Press. Vessel Technol.*, vol. 130, no. 1, pp. 011204-011204–6, Jan. 2008.

[10]Sierra Solid Mechanics Team, “Sierra/Solid Mechanics 4.48 User’s Guide,” Sandia National Laboratories, Albuquerque, NM, 2018. SAND202018-2961.

[11]Smith, J.A., “Industry practices and standards for fastener fabrication – A summary of a discussion between SNL and B&B Specialties (Anaheim, CA)”, Sandia National Laboratories, Albuquerque, NM, 2017. SAND2017-2171. *Unpublished.*